Transient Dynamics of Terrestrial Carbon Storage: Mathematical foundation and its applications

Yiqi Luo[1,2], Zheng Shi[1], Xingjie Lu[3], Jianyang Xia[4], Junyi Liang[1], Jiang Jiang[1], Ying Wang[5], Matthew J. Smith[6], Lifen Jiang[1], Anders Ahlström[7, 8], Benito Chen[9], Oleksandra Hararuk[10], Alan Hastings[11], Forrest Hoffman[12], Belinda Medlyn[13], Shuli Niu[14], Martin Rasmussen[15], Katherine Todd-Brown[16], Ying-Ping Wang[3]

[1]Department of Microbiology and Plant Biology, University of Oklahoma, Norman, Oklahoma, USA, [2]Center for Earth System Science, Tsinghua University, Beijing, China, [3]CSIRO Oceans and Atmosphere, Aspendale, Victoria, Australia, [4]School of Ecological and Environmental Sciences, East China Normal University, Shanghai, China, [5]Department of Mathematics, University of Oklahoma, Norman, Oklahoma, USA, [6]Computational Science Laboratory, Microsoft Research, Cambridge, UK, [7]Department of Earth System Science, Stanford University, Stanford, California, USA, [8]Department of Physical Geography and Ecosystem Science, Lund University, Lund, Sweden, [9]Department of Mathematics, University of Texas, Arlington, TX, USA, [10]Department of Natural Resource Sciences, McGill University, Montreal,, Canada, [11]Department of Environmental Science and Policy, University of California, One Shields Avenue, Davis, CA 95616, USA, [12]Computational Earth Sciences Group, Oak Ridge National Laboratory, Oak Ridge, TN 37831, USA, [13]Hawkesbury Institute for the Environment, Western Sydney University, Penrith NSW 2751, Australia, [14]Institute of Geographic Sciences and Natural Resources Research, Chinese Academy of Sciences, China, [15]Department of Mathematics, Imperial College, London, UK, [16]Biological Sciences Division, Pacific Northwest

National Laboratory, Richland, Washington, USA,

Running Title: Land carbon storage dynamics

Correspondence author: Yiqi Luo

Email: yluo@ou.edu

Key words Carbon cycle, carbon sequestration, dynamic disequilibrium, model intercomparison, terrestrial ecosystems, traceability analysis

Type of paper: Primary Research Article

Abstract Terrestrial ecosystems have absorbed roughly 30% of anthropogenic CO_2 emissions over the past decades, but it is unclear whether this carbon (C) sink will endure into the future. Despite extensive modeling, experimental, and observational studies, what fundamentally determines transient dynamics of terrestrial C storage under global change is still not very clear. Here we develop a new framework for understanding transient dynamics of terrestrial C storage through mathematical analysis and numerical experiments. Our analysis indicates that the ultimate force driving ecosystem C storage change is the C storage capacity, which is jointly determined by ecosystem C input (e.g., net primary production, NPP) and residence time. Since both C input and residence time vary with time, the C storage capacity is time-dependent and acts as a moving attractor that actual C storage chases. The rate of change in C storage is proportional to the C storage potential, the difference between the current storage and the storage capacity. The C storage capacity represents instantaneous responses of the land C cycle to external forcing, whereas the C storage potential represents the internal capability of the land C cycle to influence the C change trajectory in the next time step. The influence happens through redistribution of net C pool changes in a network of pools with different residence times.

Moreover, this and our other studies have demonstrated that one matrix equation can exactly replicate simulations of most land C cycle models (i.e., physical emulators). As a result, simulation outputs of those models can be placed into a three-dimensional (3D) parameter space to measure their differences. The latter can be decomposed into traceable components to track the origins of model uncertainty. In addition, the physical emulators make data assimilation computationally feasible so that both C flux- and pool-related datasets can be used to better constrain model predictions of land C sequestration. Overall, this new mathematical framework offers new approaches to understand, evaluate, diagnose, and improve land C cycle models.

1 Introduction

Terrestrial ecosystems have been estimated to sequester approximately 30% of anthropogenic carbon (C) emission in the past three decades (Canadell et al., 2007). Cumulatively, land ecosystems have sequestered more than 160 Gt C from 1750 to 2015 (Le Quéré et al., 2015). Without land C sequestration, the atmospheric CO_2 concentration would have increased by additional 95 parts per million and result in more climate warming (Le Quéré et al., 2015). During one decade from 2005 to 2014, terrestrial ecosystems sequestrated 3±0.8 Gt C per year (Le Quéré et al., 2015), which would cost billion dollars if the equivalent amount of C was sequestrated using C capture and storage techniques (Smith et al., 2016). Thus, terrestrial ecosystems effectively mitigate global change through natural processes with minimal cost. Whether this terrestrial C sequestration would endure into the future, however, is not clear, making the mitigation of global change greatly uncertain. To predict future trajectories of C sequestration in the terrestrial ecosystems, it is essential to understand fundamental mechanisms that drive terrestrial C storage dynamics.

To predict future land C sequestration, the modeling community has developed many C cycle models. According to a review by Manzoni and Porporato (2009), approximately 250 biogeochemical models have been published over a time span of 80 years to describe carbon and nitrogen mineralization. The majority of those 250 models follow some mathematical formulations of ordinary differential equations. Moreover, many of those biogeochemical models incorporate more and more processes in an attempt to simulate C cycle processes as realistically as possible (Oleson et al., 2013). As a consequence, terrestrial C cycle models have become increasingly complicated and less tractable. Almost all model intercomparison projects (MIPs), including those involved in the last three IPCC assessments, indicate that C cycle models have

consistently projected widely spread trajectories of land C sinks and were also found to fit observations poorly (Todd-Brown et al., 2013; Luo et al., 2015). The lack of progress in uncertainty analysis urges us to understand mathematical foundation of those terrestrial C models so as to diagnose causes of model spreads and improve model predictive skills.

Meanwhile, many countries have made great investments on various observational and experimental networks (or platforms) in hope to quantify terrestrial C sequestration. For example, FLUXNET has been established about 20 years ago to quantify net ecosystem exchange (NEE) between the atmosphere and biosphere (Baldocchi et al., 2001). Orbiting Carbon Observatory 2 (OCO-2) satellite was launched in 2014 to quantify carbon dioxide concentrations and distributions in the atmosphere at high spatiotemporal resolution to constrain land surface C sequestration (Hammerling et al., 2012). Networks of global change experiments have been designed to uncover processes that regulate ecosystem C sequestration (Rustad et al., 2001; Luo et al., 2011; Fraser et al., 2013; Borer et al., 2014). Massive data have been generated from those observational systems and experimental networks. They offer an unprecedented opportunity for advancing our understanding of ecosystem processes and constraining model prediction of ecosystem C sequestration. Indeed, many of those networks were initiated with one goal to improve our predictive capability. Yet the massive data have been rarely integrated into earth system models to constrain their predictions. It is a grand challenge in our era to develop innovative approaches to integration of big data into complex models so as to improve prediction of future ecosystem C sequestration.

From a system perspective, ecosystem C sequestration occurs only when the terrestrial C cycle is in a transient state, under which C influx into one ecosystem is larger than C efflux from the ecosystem. Olson (1963) is probably among the first to examine organic matter storage in

105 forest floors from the system perspective. His analysis approximated steady-state storage of
106 organic matter as a balance of litter producers and decomposers for different forest types.
107 However, global change differentially influences various C cycle processes in ecosystems and
108 results in transient dynamics of terrestrial C storage (Luo and Weng, 2011). For example, rising
109 atmospheric CO_2 concentration primarily stimulates photosynthetic C uptake while climate
110 warming likely enhances decomposition. When ecosystem C uptake increases in a unidirectional
111 trend under elevated [CO_2], terrestrial C cycle is at disequilibrium, leading to net C storage. The
112 net gained C is first distributed to different pools, each of which has a different turnover rate (or
113 residence time) before C is eventually released back to the atmosphere via respiration.
114 Distribution of net C exchange to multiple pools with different residence times is an intrinsic
115 property of an ecosystem to gradually equalize C efflux with influx (i.e. internal recovery force
116 toward an attractor). In contrast, global change factors that causes changes in C input and
117 decomposition is considered external forces that create disequilibrium through altering internal C
118 processes and pool sizes. The transient dynamics of terrestrial C cycle at disequilibrium is
119 maintained by interactions of internal processes and external forces (Luo and Weng, 2011).
120 Although the transient dynamics of terrestrial C storage have been conceptually discussed, we
121 still lack a quantitative formulation to estimate transient C storage dynamics in the terrestrial
122 ecosystems.

123 This paper was designed to address a question: what determines transient dynamics of C
124 storage in terrestrial ecosystems from a system perspective? We first reviewed the major
125 processes that most models have incorporated to simulate terrestrial C sequestration. The review
126 helps establish that terrestrial C cycle can be mathematically represented by a matrix equation.
127 We also described the Terrestrial ECOsystem (TECO) model with its numerical experiments in

support of the mathematical analysis. We then presented results of mathematical analysis on determinants of the terrestrial C storage, direction and magnitude of C storage at a given time point, and numerical experiments to illustrate climate impacts on terrestrial C storage. We carefully discussed assumptions of those terrestrial C cycle models as represented by the matrix equation, the validity of this analysis, and two new concepts introduced in this study, which are the C storage capacity and C storage potential. We also discussed the potential applications of this analysis to model uncertainty analysis and data-model integration. Moreover, we proposed that the C storage potential be a targeted variable for research, trading, and government negotiation for C credit.

2 Methods

2.1 Mathematical representation of terrestrial C cycle

This study was conducted mainly with mathematical analysis. We first established the basis of this analysis, which is that the majority of terrestrial C cycle models can be represented by a matrix equation.

Hundreds of models have been developed to simulate terrestrial C cycle (Manzoni and Porporato, 2009). All the models have to simulate processes of photosynthetic C input, C allocation and transformation, and respiratory C loss. It is well understood that photosynthesis is a primary pathway of C flow into land ecosystems. Photosynthetic C input is usually simulated according to carboxylation and electron transport rates (Farquhar et al., 1980). Ecosystem C influx varies with time and space mainly due to variations in leaf photosynthetic capacity, leaf area index of canopy, and a suite of environmental factors such as temperature, radiation, and relative humidity (or other water-related variables) (Potter et al., 1993; Sellers et al., 1996;

Keenan et al., 2012; Walker et al., 2014, Parolari and Porporato 2016).

Photosynthetically assimilated C is partly used for plant biomass growth and partly released back into the atmosphere through plant respiration. Plant biomass in leaves and fine roots usually lives for several months up to a few years before death, while woody tissues may persist for hundreds of years in forests. Dead plant materials are transferred to litter pools and decomposed by microorganisms to be partially released through heterotrophic respiration and partially stabilized to form soil organic matter (SOM). SOM can store C in the soil for hundreds or thousands of years before it is broken down to CO_2 through microbial respiration (Luo and Zhou, 2006). This series of C cycle processes has been represented in most ecosystem models with multiple pools linked by C transfers among them (Jenkinson et al., 1987; Parton et al., 1987; 1988; 1993), including those embedded in Earth system models (Ciais et al., 2013).

The majority of the published 250 terrestrial C cycle models use ordinary differential equations to describe C transformation processes among multiple plant, litter, and soil pools (Manzoni and Porporato, 2009). Those ordinary differential equations can be summarized into a matrix formula (Luo et al., 2001; 2003; Luo and Weng, 2011; Luo et al., 2015; 2016; Sierra and Müller 2015) as:

$$\begin{cases} X'(t) = Bu(t) - A\xi(t)KX(t) \\ X(t=0) = X_0 \end{cases} \quad (1)$$

where $X'(t)$ is a vector of net C pool changes at time t, $X(t)$ is a vector of pool sizes, B is a vector of partitioning coefficients from C input to each of the pools, $u(t)$ is C input rate, A is a matrix of transfer coefficients (or microbial C use efficiency) to quantify C movement along the pathways, K is a diagonal matrix of exit rates (mortality for plant pools and decomposition coefficients of litter and soil pools) from donor pools, $\xi(t)$ is a diagonal matrix of environmental scalars to represent responses of C cycle to changes in temperature, moisture, nutrients, litter

quality, and soil texture, and X_0 is a vector of initial values of pool sizes of X. In eq. 1, all the off-diagonal elements of matrix A, a_{ji}, are negative to reverse the minus sign and indicate positive C influx to the receiving pools. The equation describes net C pool change, $X'(t)$, as a difference between C input, $u(t)$, distributed to different plant pools via partitioning coefficients, B, and C loss through the C transformation matrix, $A\xi(t)K$, among individual pools, $X(t)$. Elements in vector B, matrices A and K could vary with many factors, such as vegetation types, soil texture, microbial attributes, and litter chemistry. For example, vegetation succession may influence elements in vector B, matrices A and K in addition to C input, $u(t)$, and forcing that affects C dynamics through environmental scalars, $\xi(t)$.

After synthesis of all the possible soil C cycle models based on six principles (mass balance, substrate dependence of decomposition, heterogeneity of decay rates, internal transformations of organic matter, environmental variability effects, and substrate interactions), Sierra and Müller (2015) concluded that this form of matrix equation such as eq. 1 represents the majority of terrestrial C cycle models. Similarly, Manzoni and Porporato (2009) concluded their review of 250 models that the majority of them use ordinary differential equations, which can be summarized by eq. 1, to describe land C cycle. Our mathematical analysis in this study used matrix operations of eq. 1 to reveal determinants of transient dynamics of terrestrial C cycle, including direction and rate of C storage changes, in response to global change. We examined assumptions underlying this equation and the validity of our analysis in the Discussion section.

2.2 TECO Model, its physical emulator, and numerical experiments

We conducted numerical experiments to support the mathematical analysis and thus help understand the characteristics of terrestrial C storage dynamics using the Terrestrial ECOsystem

197 (TECO) model. TECO has five major components: canopy photosynthesis, soil water dynamics,
198 plant growth, litter and soil carbon decomposition and transformation, and nitrogen dynamics as
199 described in detail by Weng and Luo (2008) and Shi et al. (2016). Canopy photosynthesis is
200 referred from a two-leaf (sunlit and shaded) model developed by Wang and Leuning (1998). This
201 submodel simulates canopy conductance, photosynthesis, and partitioning of available energy.
202 The model combines the leaf photosynthesis model developed by Farquhar et al. (1980) and a
203 stomatal conductance model (Harley et al., 1992). In the soil water dynamic submodel, soil is
204 divided into 10 layers. The surface layer is 10 cm deep and the other 9 layers are 20 cm deep.
205 Soil water content (SWC) in each layer results from the mass balance between water influx and
206 efflux. The plant growth submodel simulates C allocation and phenology. Allocation of C among
207 three plant pools, which are leaf, fine root, and wood, depends on their growth rates (Fig. 1a).
208 Phenology dynamics are related to leaf onset, which is triggered by growing degree days, and
209 leaf senescence, which is determined by temperature and soil moisture. The C transformation
210 submodel estimates carbon transfer from plants to two litter pools and three soil pools (Fig. 1a).
211 The nitrogen (N) submodel is fully coupled with C processes with one additional mineral N pool.
212 Nitrogen is absorbed by plants from mineral soil and then partitioned among leaf, woody tissues
213 and fine roots. Nitrogen in plant detritus is transferred among different ecosystem pools (i.e.
214 litter, coarse wood debris, fast, slow and passive SOM) (Shi et al., 2016). The model is driven by
215 climate data, which include air and soil temperature, vapor-pressure deficit, relative humidity,
216 incident photosynthetically active radiation, and precipitation at hourly steps.
217 We first calibrated TECO with eddy flux data collected at Harvard Forest from 2006-
218 2009. The calibrated model was spun up to the equilibrium state in pre-industrial environmental
219 conditions by recycling a 10-year climate forcing (1850-1859). Then the model was used to

simulate C dynamics from year 1850 to 2100 with the historical forcing scenario for 1850-2005 and RCP8.5 scenario for 2006-2100 as in the Community Land Model 4.5 (Oleson et al., 2013) in the grid cell where Harvard Forest is located.

To support the mathematical analysis using eq. 1, we first developed a physical emulator (i.e., the matrix representation of eq. 1) of the TECO model and then verified that the physical emulator can exactly represent simulations of the original TECO model. We first identified those parameter values in each of the C balance equations in the TECO model that are corresponding to elements in matrices A and K in eq. 1. The time-dependent variables for $u(t)$, elements in vector B, and elements in matrix $\xi(t)$ in the physical emulator were directly from outputs of the original TECO model. Then those parameter values and time-dependent variables were organized into matrices A, $\xi(t)$, and K; vectors $X(t)$, X_0, and B; and variable $u(t)$. Note that values of $u(t)$, B, and $\xi(t)$ could be different among different climate scenarios. Those matrices, vectors, and variable were entered to matrix calculation to compute $X'(t)$ using eq. 1. The sum of elements in calculated $X'(t)$ is a 100% match with simulated net ecosystem production (NEP) with the TECO model (Fig. 1b).

Once eq. 1 was verified to exactly replicate TECO simulations, we used TECO to generate numerical experiments to support the mathematical analysis on the transient dynamics of terrestrial C storage. To analyze the seasonal patterns of C storage dynamics, we averaged 10 series of three-year seasonal dynamics from 1851-1880. Then we used a 7-day moving window to further smooth the data.

3. Results

3.1 Determinants of C storage dynamics

The transient dynamics of terrestrial carbon storage are determined by two components: the C storage capacity and the C storage potential. The two components of C storage dynamics can be mathematically derived from multiplying both sides of eq. 1 by $(A\xi(t)K)^{-1}$ as:

$$X(t) = (A\xi(t)K)^{-1}Bu(t) - (A\xi(t)K)^{-1}X'(t) \quad (2)$$

The first term on the right side of eq. 2 is the C storage capacity and the second term is the C storage potential. Fig. 2a shows time courses of C storage and its capacity over one year for the leaf pool of Harvard Forest.

In eq. 2, we name the term $(A\xi(t)K)^{-1}$ the chasing time, $\tau_{ch}(t)$, with a time unit used in exit rate K. The chasing time is defined as:

$$\tau_{ch}(t) = (A\xi(t)K)^{-1} \quad (3)$$

$\tau_{ch}(t)$ is a matrix of C residence times through the network of individual pools each with a different residence time and fractions of received C connected by pathways of C transfer. Analogous to the fundamental matrix measuring life expectancies in demographic models (Caswell, 2000), the matrix, $\tau_{ch}(t)$, here measures expected residence time of a C atom in pool *i* when it has entered from pool *j*. We call this matrix the fundamental matrix of chasing times to represent the time scale at which the net C pool change, $X'(t)$, is redistributed in the network. Meanwhile, the residence times of individual pools in network, $\tau_N(t)$, can be estimated by multiplying the fundamental matrix of chasing times, $(A\xi(t)K)^{-1}$, with a vector of partitioning coefficients, *B* as:

$$\tau_N(t) = (A\xi(t)K)^{-1}B \quad (4a)$$

Ecosystem residence time, $\tau_E(t)$, is the sum of the residence time of all individual pools in network as:

$$\tau_E(t) = (1 \quad 1 \quad \cdots \quad 1)\tau_N(t) \tag{4b}$$

Thus, the C storage capacity can be defined by:

$$X_c(t) = (A\xi(t)K)^{-1}Bu(t) \tag{5a}$$

Or it can be estimated from C input, $u(t)$, and residence time, $\tau_N(t)$, as:

$$X_C(t) = \tau_N(t)u(t) \tag{5b}$$

As C input (e.g., Gross or Net Primary Productions, GPP or NPP) and residence times vary with time, the C storage capacity varies with time. It represents instantaneous responses of the terrestrial C cycle to the external forcing. The modeled C storage capacity in the leaf pool (Fig. 2a), for example, increases in spring, reaches the peak at summer, declines in autumn, and becomes minimal in winter largely due to strong seasonal changes in C input (Fig. 2b). Note that either GPP or NPP can be used as C input for analysis of transient C dynamics. Estimated residence times, however, are smaller with GPP as C input than those with NPP as input. In this paper, we mostly used NPP as C input as that fraction of C is distributed among pools.

The C storage potential at time *t*, $X_p(t)$, can be mathematically described as:

$$X_p(t) = (A\xi(t)K)^{-1}X'(t) \tag{6a}$$

Or it can be estimated from net C pool change, $X'(t)$, and chasing time, $\tau_{ch}(t)$ as:

$$X_p(t) = \tau_{ch}(t)X'(t) \tag{6b}$$

Eqs. 6a and 6b suggest that the C storage potential represents re-distribution of net C pool change, $X'(t)$, of individual pools through a network of pools with different residence times as connected by C transfers from one pool to the others through all the pathways. As time evolves, the net C pool change, $X'(t)$, is redistributed again and again through the network of pools. The network of redistribution of next C pool change, thus, represents the potential of an ecosystem to store additional C when it is positive and lose C when it is negative. The C storage potential can

289 also be estimated from the difference between the C storage capacity and the C storage itself at
290 time *t* as:

291 $$X_p(t) = X_c(t) - X(t) \quad (6c)$$

292 The C storage potential in the leaf pool, for example, is about zero in winter and early spring
293 when the C storage capacity is very close to the storage itself (Fig. 2a). The C storage potential is
294 positive when the capacity is larger than the storage itself from late spring to summer and early
295 fall. As the storage capacity decreases to the point when the storage equals the capacity on the
296 265th day of year (DOY), the C storage potential is zero. After that day, the C storage potential
297 becomes negative.

298 Dynamics of ecosystem C storage, $X(t)$, can be characterized by three parameters: C
299 influx, $u(t)$, residence times, $\tau_N(t)$, and the C storage potential $X_p(t)$ as:

300 $$X(t) = \tau_N(t)u(t) - X_p(t) \quad (7)$$

301 Eq. 7 represents a three-dimensional (3D) parameter space within which model simulation
302 outputs can be placed to measure how and how much they diverge.

303 Note that sums of elements in vectors $X(t)$, $X_c(t)$, $X_p(t)$, and $X'(t)$ are corresponding,
304 respectively, to the whole ecosystem C stock, ecosystem C storage capacity, ecosystem C storage
305 potential, and net ecosystem production (NEP). In this paper, we describe them wherever
306 necessary rather than use a separate set of symbols to represent those sums.

307

308 **3.2 Direction and rate of C storage change at a given time**

309 Like studying any moving object, quantifying dynamics of land C storage needs to determine
310 both the direction and the rate of its change at a given time. To determine the direction and rate
311 of C storage change, we re-arranged eq. 2 to be:

$$\tau_{ch} X'(t) = X_c(t) - X(t) = X_p(t) \quad (8a)$$

or re-arranging eq. 6a leads to:

$$X'(t) = A\xi(t)KX_p(t) \quad (8b)$$

As all the elements in τ_{ch} are positive, the sign of $X'(t)$ is the same as for $X_p(t)$. That means $X'(t)$ increases when $X_c(t) > X(t)$, does not change when $X_c(t) = X(t)$, and decreases when $X_c(t) < X(t)$ at the ecosystem scale. Thus, the C storage capacity, $X_c(t)$, is an attractor and hence determines the direction toward which the C storage, $X(t)$, chases at any given time point. The rate of C storage change, $X'(t)$, is proportional to $X_p(t)$ and also regulated by τ_{ch}.

When we study C cycle dynamics, we are interested in understanding dynamics of not only a whole ecosystem but also individual pools. Eq. 8a can be used to derive equations to describe C storage change for an i^{th} pool as:

$$\sum_{j=1}^{n} f_{ij}\, \tau_i\, x'_j(t) = \sum_{j=1}^{n} f_{ij}\, \tau_i b_j u(t) - x_i(t) = x_{p,i}(t) \quad (9a)$$

where n is the number of pools in a C cycle model, f_{ij} is a fraction of C transferred from pool j to i through all the pathways, τ_i measures residence times of individual pools in isolation (in contrast to τ_N in the network), x'_j is the net C change in the j^{th} pool, b_j is a partitioning coefficient of C input to the j^{th} pool, $x_i(t)$ is the C storage in the i^{th} pool, and $x_{p,i}(t)$ is the C storage potential in the i^{th} pool. Eq. 9a means that the C storage potential of each pool at time t, $x_{p,i}(t)$, is the sum of all the individual net C pool change, x'_j, multiplied by corresponding residence time spent in pool i coming from pool j. Through re-arrangement, eq. 9a can be solved for each individual pool net C change as a function of C storage potential of all the pools as:

$$x'_i(t) = \frac{x_{c,i,u}(t) - x_{c,i,p}(t) - x_i(t)}{f_{ii}\tau_i} \quad (9b)$$

where $x_{c,i,u}(t) = \sum_{j=1}^{n} f_{ij}\,\tau_i b_j u(t)$ for the maximal amount of C that can transfer from C input to the i[th] pool. $x_{c,i,p}(t) = \sum_{j=1,j\neq i}^{n} f_{ij}\,\tau_i x'_j(t)$ for the maximal amount of C that can transfer from all the other pools to the i[th] pool. $f_{ii} = 1$ for all the pools if there is no feedback of C among soil pools. $f_{ii} < 1$ when there are feedbacks of C among soil pools.

As plant pools get C only from photosynthetic C input, $u(t)$, but not from other pools, the direction and rate of C storage change in the i[th] plant pool is determined by:

$$\begin{cases} x'_i(t) = \frac{x_{c,i}(t) - x_i(t)}{\tau_i} = \frac{X_{p,i}(t)}{\tau_i} \\ x_{c,i}(t) = b_i u(t)\tau_i \end{cases} \quad \text{for i = 1, 2, 3} \qquad (10)$$

The C storage capacity of plant pools equals the product of plant C input, $u(t)$ (i.e., net primary production, NPP), partitioning coefficient, b_i, and residence time, τ_i, of its own pool (Fig. 2b-d). Thus, the C storage capacities of the leaf, root, and wood pools are high in summer and low in winter. Plant C storage, $x_i(t)$, still chases the storage capacity, $x_{c,i}(t)$, of its own pool at a rate that is proportional to $X_{p,i}(t)$. For the leaf pool, the C storage, $x_1(t)$, increases when $x_{c,1}(t) > x_1(t)$ (or $x_{p,1}(t)>0$) from late spring until early fall on the 265[th] day of year (DOY) and then decreases when $x_{c,1}(t) < x_1(t)$ (or $x_{p,1}(t)<0$) from DOY of 265 until 326 during fall (Fig. 2a).

However, the direction of C storage change in litter and soil pools are no longer solely determined by the storage capacity, $x_{c,i}(t)$, of their own pools or at a rate that is proportional to $X_{p,i}(t)$. The C storage capacity of one litter or soil pool has two components. One component, $x_{c,i,u}(t)$ is set by the amount of plant C input, $u(t)$, going through all the possible pathways, $f_{ij}b_j$, multiplied by residence time, τ_i, of its own pool. The second component measures the C exchange of one litter or soil pool with other pools according to net C pool change, $x'_j(t)$, through pathways, $f_{ij}, j \neq i$, weighed by residence time, τ_i, of its own pool. For example, C input to the litter pool is a combination of C transfer from C input through the leaf, root, and

wood pools (Fig. 3c, 3d, and 3e) and C transfer due to the net C pool changes in the leaf, root, and wood pools (Fig. 3f, 3g, and 3h). Thus the first capacity component of the litter pool to store C is the sum of three products of NPP, C partitioning coefficient, and network residence time, respectively, through the leaf, root, and wood pools (Fig. 3c, 3d, and 3e). The second capacity component is the sum of other three products of C transfer coefficient along all the possible pathways, network residence time, and net C pool changes, respectively, in the leaf, root, and wood pools (Fig. 3f, 3g, and 3h). Thus, C storage in the i^{th} pool, $x_i(t)$, chases an attractor, $(\sum_{j=1}^{n} f_{ij}\, b_j u(t) - \sum_{j=1, j\neq i}^{n} f_{ij}\, \tau_i x'_j(t))\tau_i$, for litter and soil pools (Fig. 4).

In summary, due to the network of C transfer, C storage in litter and soil pools does not chase the C storage capacities of their own pools in a multiple C pool model (Fig. 4). The capacities for individual litter and soil pools measure the amounts of C that is transferred from photosynthetic C input through plant pools to be stored in those pools. However, those litter and soil pools also exchange C with other pools according to transfer coefficients along pathways of C movement multiplying net C pool change in those pools. Integration of the C input and C exchanges together still sets as a moving attractor toward which individual pool C storage approaches (Fig. 4).

3.3 C storage dynamics under global change

In response to a global change scenario that combines historical change and simulated RCP8.5 in the TECO experiment, the modeled ecosystem C storage capacity (the sum of all elements in vector $X_c(t)$) at Harvard Forest increases from 27 kg C m^{-2} in 1850 to approximately 38 kg C m^{-2} in 2100 with strong interannual variability (Fig. 5a). The increasing capacity results from a combination of a nearly 44% increase in NPP with a ~2% decrease in ecosystem residence times

(the sum of all elements in vector $\tau_E(t)$) during that period (Fig. 5b). The strong interannual variability in the modeled capacity is attributable to the variability in NPP and residence times, both of which directly respond to instantaneous variations in environmental factors. In comparison, the ecosystem C storage (the sum of all elements in vector $X(t)$) itself gradually increases, lagging behind the capacity, with much dampened interannual variability (Fig. 5a). The dampened interannual variability is due to smoothing effects of pools with various residence times. In response to global change scenario RCP8.5, the ecosystem C storage potential (the sum of all elements in vector $X_p(t)$) in the Harvard Forest ecosystem increases from zero at 1980 to 3.5 kg C m^{-2} in 2100 with strong fluctuation over years (Fig. 5a). Over seasons, the potential is high during the summer and low in winter, similarly with the seasonal cycle of the C storage capacity.

Since chasing time, τ_{ch}, is a matrix and net C pool change, $X'(t)$, is a vector, eq. 6a or 6b (i.e., the C storage potential) can not be analytically separated into the chasing time and net C pool change as can the capacity into C input and residence time in eq. 5a or 5b for traceability analysis. The relationships among the three quantities can be explored by regression analysis. The ecosystem C storage potential fluctuates in a similar phase with NEP from 1850 to 2100 (Fig. 5c). Consequently, the C storage potential is well correlated with NEP at the whole ecosystem scale (Fig. 5d). The slope of the regression line is a statistical representation of ecosystem chasing time. In this study, we find that r^2 of the relationship between the storage potential and NEP is 0.79. The regression slope is 28.1 years in comparison with the ecosystem residence time of approximately 22 years (Fig. 5b).

The capacity and storage itself of individual pools display similar long-term trends and interannual variability to those for the total ecosystem C storage dynamics (Fig. 6). Noticeably,

401 the deviation of the C storage from the capacity, which is the C storage potential, is much larger
402 for pools with long residence times than those with short residence times. For individual pools,
403 the potential is nearly zero for those fast turnover pools and becomes very large for those pools
404 with long residence time (Fig. 6).

405 For individual plant pools, eq. 10 describes the dependence of the C storage potential,
406 $x_{p,i}(t)$, on the pool-specific residence time, τ_i, i = 1, 2, and 3, and net C pool change of their
407 own pools, $x'_i(t), i$ = 1, 2, and 3. Thus, one value of $x_{p,i}(t)$ is exactly corresponding to one
408 value of $x'_i(t)$ at slope of τ_i, leading to the correlation coefficient in Fig. 7 being 1.00 for leaf,
409 root, and wood pools. For a litter or soil pool, however, the C storage potential is not solely
410 dependent on the residence time and net C pool change of its own pool but influenced by several
411 other pools. Thus, the potential of one litter or soil pool is correlated with net C pool changes of
412 several pools with different regression slopes (Fig. 7).

413

414 **4 Discussion**

415 4.1 Assumptions of the C cycle models and validity of this analysis

416 This analysis is built upon eq. 1, which represents the majority of terrestrial C cycle
417 models developed in the past decades (Manzoni and Porporato, 2009; Sierra and Müller, 2015).
418 Those models have several assumptions, which may influence the validity of this analysis. First,
419 those models assume that donor pools control C transfers among pools and decomposition
420 follows 1st-order decay functions (Assumption 1). This assumption is built upon observations
421 from litter and SOC decomposition. Analysis of data from nearly 300 studies of litter
422 decomposition (Zhang et al., 2008), about 500 studies of soil incubation (Schädel et al., 2014;
423 Xu et al., 2016), more than 100 studies of forest succession (Yang et al., 2011), and restoration

(Matamala et al., 2008) almost all suggests that the 1st-order decay function captures macroscopic patterns of land C dynamics. Even so, its biological, chemical and physical underpinnings need more study (Luo et al., 2016). This assumption has recently been challenged by a notion that microbes are actively involved in decomposition processes. To describe the active roles of microbes in organic C decomposition, a suite of nonlinear microbial models has been proposed using Michaelis-Menten or reverse Michaelis-Menten equations (Allison et al., 2010; Wieder et al., 2013). Those nonlinear models exhibit unique behaviors of modeled systems, such as damped oscillatory responses of soil C dynamics to small perturbations and insensitivity of the equilibrium pool sizes of litter or soil carbon to inputs (Li et al., 2014; Wang et al., 2014; 2016). Oscillations have been documented for single enzymes at timescales between 10^{-4} to 10 seconds (English et al., 2006; Goldbeter, 2013; Xie, 2013). Over longer timescales with mixtures of large diversity of enzyme-substrate complexes in soil, oscillations may be likely averaged out so that the 1st order decay functions may well approximate these average dynamics of organic matter decomposition (Sierra and Müller, 2015).

Second, those models all assume that multiple pools can adequately approximate transformation, decomposition, and stabilization of SOC in the real world (Assumption 2). The classic SOC model, CENTURY, uses three conceptual pools, active, slow, and passive SOC, to represent SOC dynamics (Parton et al., 1987). Several models define pools that are corresponding to measurable SOC fractions to match experimental observation with modeling analysis (Smith et al., 2002; Stewart et al., 2008). Carbon transformation in soil over time has also been described by a partial differential function of SOM quality (Bosatta and Ågren, 1991; Ågren and Bosatta, 1996). The latter quality model describes the external inputs of C with certain quality, C loss due to decomposition, and the internal transformations of the quality of

447 soil organic matter. It has been shown that multi-pool models can approximate the partial
448 differential function or continuous quality model as the number of pools increases (Bolker et al.,
449 1998; Sierra and Müller, 2015).

450 Assumption 3 is on partitioning coefficients of C input (i.e., elements in vector *B*) and C
451 transformation among plant, litter, and soil pools (i.e., elements in the matrix, $A\xi(t)K$). Some of
452 the terrestrial C cycle models assume that elements in vector *B*, and matrices *A* and *K* are
453 constants. All the factors or processes that vary with time are represented in the diagonal matrix
454 $\xi(t)$. In the real world, C transformation are influenced by environmental variables (e.g.,
455 temperature, moisture, oxygen, N, phosphorus, and acidity varying with soil profile, space, and
456 time), litter quality (e.g., lignin, cellulose, N, or their relative content), organomineral properties
457 of SOC (e.g., complex chemical compounds, aggregation, physiochemical binding and
458 protection, reactions with inorganic, reactive surfaces, and sorption), and microbial attributes
459 (e.g., community structure, functionality, priming, acclimation, and other physiological
460 adjustments) (Luo et al., 2016). It is not practical to incorporate all of those factors and processes
461 into one model. Only a subset of them is explicitly expressed while the majority is implicitly
462 embedded in the C cycle models. Empirical studies have suggested that temperature, moisture,
463 litter quality, and soil texture are primary factors that control C transformation processes of
464 decomposition and stabilization (Burke et al., 1989; Adair et al., 2008; Zhang et al., 2008; Xu et
465 al., 2012; Wang et al., 2013). Nitrogen influences C cycle processes mainly through changes in
466 photosynthetic C input, C partitioning, and decomposition. It is yet to identify how other major
467 factors and processes, such as microbial activities and organomineral protection, regulate C
468 transformation.

Assumption 4 is that terrestrial C cycle models use different response functions (i.e., different $\xi(t)$ in eq. 1) to represent C cycle responses to external variables. As temperature modifies almost all processes in the C cycle, different formulations, including exponential, Arrhenius, and optimal response functions, have been used to describe C cycle responses to temperature changes in different models (Lloyd and Taylor, 1994; Jones et al., 2005; Sierra and Müller, 2015). Different response functions are used to connect C cycle processes with moisture, nutrient availability, soil clay content, litter quality, and other factors. Different formulations of response functions may result in substantially different model projections (Exbrayat et al., 2013) but unlikely change basic dynamics of the model behaviors.

Assumption 5 is that disturbance events are represented in models in different ways (Grosse et al., 2011; West et al., 2011; Goetz et al., 2012; Hicke et al., 2012). Fire, extreme drought, insect outbreaks, land management, and land cover and land use change influence terrestrial C dynamics via 1) altering rate processes, for example, gross primary productivity (GPP), growth, tree mortality, or heterotrophic respiration; 2) modifying microclimatic environments; 3) transferring C from one pool to another (e.g., from live to dead pools during storms or release to the atmosphere with fire) (Kloster et al., 2010; Thonicke et al., 2010; Luo and Weng, 2011; Prentice et al., 2011; Weng et al., 2012). Those disturbance influences can be represented in terrestrial C cycle models through changes in parameter values, environmental scalars, and/or discrete C transfers among pools of eq. 1 (Luo and Weng 2011). While eq. 1 does not explicitly incorporate disturbances for their influences on land C cycle, Weng et al. (2012) developed a disturbance regime model that combines eq. 1 with frequency distributions of disturbance severity and intervals to quantify net biome exchanges.

The sixth assumption that those models make is that the lateral C fluxes through erosion

or local C drainage is negligible so that eq (1) can approximate terrestrial C cycle over space. If soil erosion is substantial enough to be modeled with horizontal movement of C, a third dimension should be added in addition to two-dimensional transfers in classic models.

Our analysis on transient dynamics of terrestrial C cycle is valid unless some of the assumptions are violated. Assumption 1 on the 1st-order decay function of decomposition appears to be supported by thousands of datasets. It is a burden on microbiologists to identify empirical evidence to support the nonlinear microbial models. Assumption 2 may not affect the validity of our analysis no matter how C pools are divided in the ecosystems. Our analysis in this study is applicable no matter whether elements are time-varying or constant in vector B and matrices A and K as in assumption 3. Neither assumption 4 nor 5 would affect the analysis in this study. The environmental scalar, $\xi(t)$, as related to assumption 4 can be any forms in the derived equations (e.g., eq. 2). Disturbances of fire, land use, and extreme drought change rate processes but do not alter the basic formulation of eq. 1. If soil erosion and lateral transportation of C become a major research objective, Eq. (1) can no longer be analyzed to understand the mathematical foundation underlying transient dynamics of terrestrial C cycle.

4.2 Carbon storage capacity

One of the two components this analysis introduces to understand transient dynamics of terrestrial C storage is the C storage capacity (Eq. 2). Olson (1963) is probably among the first who systematically analyzed C storage dynamics at forest floor as functions of litter production and decomposition. He collected data of annual litter production and approximately steady-state organic C storage at forest floor, from which decomposition rates were estimated for a variety of ecosystems from Ghana in the tropics to alpine forests in California. Using the relationships

among litter production, decomposition, and C storage, Olson (1963) explored several issues, such as decay without input, accumulation with continuous or discrete annual litter fall, and adjustments in production and decay parameters during forest succession. His analysis approximated the steady-state C storage as the C input times the inverse of decomposition (i.e., residence time). The steady-state C storage is also considered the maximal amount of C that a forest can store.

This study is not only built upon Olson's analysis but also expands it at least in two aspects. First, we similarly define the C storage capacity (i.e., eqs. 5a and 5b). Those equations can be applied to a whole ecosystem with multiple C pools while Olson's analysis is for one C pool. Second, Olson (1963) treated the C input and decomposition rate as yearly constants at a given location even though they varied with locations. This study considers both C input and rate of decomposition being time dependent. A dynamical system with its input and parameters being time dependent mathematically becomes a nonautonomous system (Kloeden and Rasmussen, 2011). As terrestrial C cycle under global change is transient, we need to treat it a nonautonomous system to better understand the properties of transient dynamics. Olson (1963) approximated the non-autonomous system at the yearly time scale without global change so as to effectively understand properties of the steady-state C storage at the forest floor. In comparison, eqs. 5a and b are not only more general but also essential for understanding transient dynamics of the terrestrial C cycle in response to global change.

Under the transient dynamics, the C storage capacity as defined by eqs 5a and b still sets the maximal amount of C that one ecosystem can store at time t. This capacity represents instantaneous responses of ecosystem C cycle to external forcing via changes in both C input and residence time, and thus varies within one day, over seasons of a year, and interannually over

538 longer time scales as forcings vary. The variation of the C storage capacity can result from cyclic
539 environmental changes (e.g., dial and seasonal changes), directional global change (e.g., rising
540 atmospheric CO_2, nitrogen deposition, altered precipitation, and warming), disturbance events,
541 disturbance regime shifts, and changing vegetation dynamics (Luo and Weng, 2011). As the
542 capacity sets the maximal amount of C storage (Fig. 2a), it is a moving attractor toward which
543 the current C storage chases. When the capacity is larger than the C storage itself, C storage
544 increases. Otherwise, the C storage decreases.
545
546 **4.3 Carbon storage potential**
547 The C storage potential represents the internal capability to equilibrate the current C storage with
548 the capacity. Bogeochemically, the C storage potential represents re-distribution of net C pool
549 change, $X'(t)$, of individual pools through a network of pools with different residence times as
550 connected by C transfers from one pool to the others through all the pathways. The potential is
551 conceptually equivalent to the magnitude of disequilibrium as discussed by Luo and Weng
552 (2011).
553 Extensive studies have been done to quantify terrestrial C sequestration. The most
554 commonly estimated quantities for C sequestration include net ecosystem exchange (NEE), C
555 stocks in ecosystems (i.e., plant biomass and SOC) and their changes (Baldocchi et al., 2001; Pan
556 et al., 2013). This study, for the first time, offers the theoretical basis to estimate the terrestrial C
557 storage potential in at least two approaches: (1) the product of chasing time and net C pool
558 change with eqs. 6a and 6b; and (2) the difference between the C storage capacity and the C
559 storage itself with eqs. 6c. Since the time-varying C storage capacity is fully defined by
560 residence time and C input at any given time, C storage potential can be estimated from three

quantities: C input, residence time, and C storage.

To effectively quantify the C storage potential in terrestrial ecosystems, we need various data sets from experimental and observatory studies to be first assimilated into models. For example, data from Harvard Forest were first used to constrain the TECO model. The constrained model was used to explore changes in ecosystem C storage in response to global change scenario, RCP8.5. That scenario primarily stimulated NPP, which increased from 1.06 to 1.8 kg C m^{-2} yr^{-1} in the Harvard Forest (Fig. 5b). Although climate warming decreased residence time in the Harvard Forest, the substantial increases in NPP resulted in increases in the C storage potential over time.

4.4 Novel approaches to model evaluation and improvement

Our analysis of transient C cycle dynamics offers new approaches to understand, evaluate, diagnose, and improve land C cycle models. We have demonstrated that many global land C cycle models can be exactly represented by the matrix equation (Eqs. 1 and 2) (i.e., physical emulators). As a consequence, outputs of all those models can be placed into a three dimensional (3D) space (Eq. 7) to measure their differences. In addition, components of land C cycle models are simulated in a mutually independent fashion so that modeled C storage can be decomposed into traceable components for traceability analysis. Moreover, the physical emulators computationally enable data assimilation to constrain complex models.

Physical Emulators of land C cycle models We have developed matrix representations (i.e., physical emulators) of CABLE, LPJ-GUESS, CLM3.5, CLM 4.0, CLM4.5, BEPS, and TECO (Xia et al., 2013; Hararuk et al., 2014; Ahlström et al., 2015; Chen et al., 2015). The emulators can exactly replicate simulations of C pools and fluxes with their original models

584 when driven by a limited set of inputs from the full model (GPP, soil temperature, and soil
585 moisture) (Fig. 1b and 1c). However, the physical emulators differ for different models as the
586 elements of each matrix could be differently parameterized or formulized in different models.
587 Also, different models usually have different pool-flux structures, leading to different non-zero
588 elements in the *A* matrix. Nonetheless, the physical emulators make complex models analytically
589 clear and, therefore, give us a way to understand the effects of forcing, model structures, and
590 parameters on modeled ecosystem processes. They greatly simplify the task of understanding the
591 dynamics of submodels and interactions between them. The emulators allow us to analyze model
592 results in the 3D parameter space and the traceability framework.

593 *Parameter space of C cycle dynamics* Eq. 7 indicates that transient dynamics of modeled
594 C storage are determined by three parameters: C input, residence time, and C storage potential.
595 The 3D parameter space offers one novel approach to uncertainty analysis of global C cycle
596 models. As global land models incorporate more and more processes to simulate C cycle
597 responses to global change, it becomes very difficult to understand or evaluate complex model
598 behaviors. As such, differences in model projections cannot be easily diagnosed and attributed to
599 their sources (Chatfield, 1995; Friedlingstein et al., 2006; Luo et al., 2009). Eq. 7 can help
600 diagnose and evaluate complex models by placing all modeling results within one common
601 parameter space in spite of the fact that individual global models may have tens or hundreds of
602 parameters to represent C cycle processes as affected by many abiotic and biotic factors (Luo et
603 al., 2016). The 3D space can be used to measure how and how much the models diverge.

604 *Traceability analysis* The two terms on the right side of eq. 2 can be decomposed into
605 traceable components (Xia et al., 2013) so as to identify sources of uncertainty in C cycle model
606 projections. Model intercomparison projects (MIPs) all illustrate great spreads in projected land

607 C sink dynamics across models (Todd-Brown et al., 2013; Tian et al., 2015). It has been
608 extremely challenging to attribute the uncertainty to sources. Placing simulation results of a
609 variety of C cycle models within one common parameter space can measure how much the
610 model differences are in a common metrics (Eq. 7). The measured differences can be further
611 attributed to sources in model structure, parameter, and forcing fields with traceability analysis
612 (Xia et al., 2013; Rafique et al., 2014; Ahlström et al., 2015; Chen et al., 2015). The traceability
613 analysis also can be used to evaluate effectiveness of newly incorporated modules into existing
614 models, such as adding the N module on simulated C dynamics (Xia et al., 2013) and locate the
615 origin of model ensemble uncertainties to external forcing vs. model structures and parameters
616 (Ahlström et al., 2015).
617 *Constrained estimates of terrestrial C sequestration* Traditionally, global land C sink is
618 indirectly estimated from airborne fraction of C emission and ocean uptake. Although many
619 global land models have been developed to estimate land C sequestration, a variety of MIPs
620 indicate that model predictions widely vary among them and do not fit observations well
621 (Schwalm et al., 2010; Luo et al., 2015; Tian et al., 2015). Moreover, the prevailing practices in
622 the modeling community, unfortunately, may not lead to significant enhancements in our
623 confidence on model predictions. For example, incorporating an increasing number of processes
624 that influence the C cycle may represent the real-world phenomena more realistically but makes
625 the models more complex and less tractable. MIPs have effectively revealed the extent of the
626 differences between model predictions (Schwalm et al., 2010; Keenan et al., 2012; De Kauwe et
627 al., 2013) but provide limited insights into sources of model differences (but see Medlyn et al.
628 2015). The physical emulators make data assimilation computationally feasible for global C
629 cycle models (Hararuk *et al*. 2014; 2015) and thus offer the possibility to generate independent

630 yet constrained estimates of global land C sequestration to be compared with the indirect
631 estimate from the airborne fraction of C emission and ocean uptake. With the emulators, we can
632 assimilate most of the C flux- and pool-related datasets into those models to better constrain
633 global land C sink dynamics.
634
635 **5 Concluding remarks**
636 In this study we theoretically explored the transient dynamics of terrestrial C storage. Our
637 analysis indicates that transient C storage dynamics can be partitioned into two components: the
638 C storage capacity and the C storage potential. The capacity, which is the product of C input and
639 residence time, represents their instantaneous responses to a state of external forcing at a given
640 time. Thus, the C storage capacity quantifies the maximum amount of C that an ecosystem can
641 store at the given environmental condition at a point of time. Thus it varies diurnally, seasonally,
642 and interannually as environmental condition changes.
643 The C storage potential is the difference between the capacity and the current C storage
644 and thus measures the magnitude of disequilibrium in the terrestrial C cycle (Luo and Weng,
645 2011). The storage potential represents the internal capability (or recovery force) of the
646 terrestrial C cycle to influence the change in C storage in the next time step through
647 redistribution of net C pool changes in a network of multiple pools with different residence
648 times. The redistribution drives the current C storage towards the capacity and thus equilibrates
649 C efflux with influx.
650 The two components of land C storage dynamics represent interactions of external forces
651 (via changes in the capacity) and internal capability of the land C cycle (via changes in the C
652 storage potential) to generate complex phenomena of C cycle dynamics, such as fluctuations,

653 directional changes, and tipping points, in the terrestrial ecosystems. From a system perspective,
654 these complex phenomena could not be generated by relatively simple internal processes but are
655 mostly caused by multiple environmental forcing variables interacting with internal processes
656 over different temporal and spatial scales as explained by Luo and Weng (2011) and Luo et al.
657 (2015). Note that while those internal processes can be mathematically represented with a
658 relatively simple formula, their ecological and biological underpinnings can be very complex.
659 The theoretical framework developed in this study has the potential to revolutionize
660 model evaluation. Our analysis indicates that the matrix equation as in eq. 1 or 2 can adequately
661 emulate most of the land C cycle models. Indeed, we have developed physical emulators of
662 several global land C cycle models. In addition, predictions of C dynamics with complex land
663 models can be placed in a 3D parameter space as a common metric to measure how much model
664 predictions are different. The latter can be traced to its source components by decomposing
665 model predictions to a hierarchy of traceable components. Moreover, the physical emulators
666 make it computationally possible to assimilate multiple sources of data to constrain predictions
667 of complex models.
668 The theoretical framework we developed in this study can well explain dynamics of C
669 storage in response to cyclic seasonal change in external forcings (e.g., Figs. 2 and 3), climate
670 change, and rising atmospheric CO_2 (Fig. 5). It can also explain responses of ecosystem C
671 storage to disturbances and other global change factors, such as nitrogen deposition, land use
672 changes, and altered precipitation. The theoretical framework is simple and straightforward but
673 able to characterize the direction and rate of C storage change, which are arguably among the
674 most critical issues for quantifying terrestrial C sequestration. Future research should explicitly
675 incorporate stochastic disturbance regime shifts (e.g., Weng et al., 2012) and vegetation

dynamics (Moorcroft et al., 2001; Purves and Pacala, 2008; Fisher et al., 2010; Weng et al., 2015) into this theoretical framework to explore their theoretical issues related to biogeochemistry.

6 Code availability

Computer code of the TECO model and its physical emulator are available at http://ecolab.ou.edu/download/TECO%20Emulator.php

Acknowledgements: This work was partially done through the working group, Nonautonomous Systems and Terrestrial Carbon Cycle, at the National Institute for Mathematical and Biological Synthesis, an institute sponsored by the National Science Foundation, the US Department of Homeland Security, and the US Department of Agriculture through NSF award no. EF-0832858, with additional support from the University of Tennessee, Knoxville. Research in Yiqi Luo EcoLab was financially supported by U.S. Department of Energy grants DE-SC0006982, DE-SC0008270, DE-SC0014062, DE-SC0004601, and DE-SC0010715 and U.S. National Science Foundation (NSF) grants DBI 0850290, EPS 0919466, DEB 0840964, and EF 1137293.

References

Adair, E. C., Parton, W. J., Del Grosso, S. J., Silver, W. L., Harmon, M. E., Hall, S. A., Burke, I. C., and Hart, S. C.: Simple three-pool model accurately describes patterns of long-term litter decomposition in diverse climates, Global Change Biol, 14, 2636-2660, 2008.

Ågren, G. I. and Bosatta, E.: Quality: A bridge between theory and experiment in soil organic matter studies, Oikos, 76, 522-528, 1996.

700 Ahlström, A., Xia, J. Y., Arneth, A., Luo, Y. Q., and smith, B.: Importance of vegetation
701 dynamics for future terrestrial carbon cycling, Environmental Research Letters, 10, 054019
702 doi:054010.051088/051748-059326/054010/054015/054019, 2015.

703 Allison, S. D., Wallenstein, M. D., and Bradford, M. A.: Soil-carbon response to warming
704 dependent on microbial physiology, Nat Geosci, 3, 336-340, 2010.

705 Baldocchi, D., Falge, E., Gu, L. H., Olson, R., Hollinger, D., Running, S., Anthoni, P.,
706 Bernhofer, C., Davis, K., Evans, R., Fuentes, J., Goldstein, A., Katul, G., Law, B., Lee, X. H.,
707 Malhi, Y., Meyers, T., Munger, W., Oechel, W., U, K. T. P., Pilegaard, K., Schmid, H. P.,
708 Valentini, R., Verma, S., Vesala, T., Wilson, K., and Wofsy, S.: FLUXNET: A new tool to study
709 the temporal and spatial variability of ecosystem-scale carbon dioxide, water vapor, and energy
710 flux densities, B Am Meteorol Soc, 82, 2415-2434, 2001.

711 Bolker, B. M., Pacala, S. W., and Parton, W. J.: Linear analysis of soil decomposition: Insights
712 from the century model, Ecol Appl, 8, 425-439, 1998.

713 Borer, E. T., Harpole, W. S., Adler, P. B., Lind, E. M., Orrock, J. L., Seabloom, E. W., and
714 Smith, M. D.: Finding generality in ecology: a model for globally distributed experiments,
715 Methods in Ecology and Evolution, 5, 65-73, 2014.

716 Bosatta, E. and Ågren, G. I.: Dynamics of carbon and nitrogen in the organic matter of the soil: a
717 generic theory, American Naturalist, 1991. 227-245, 1991.

718 Burke, I. C., Yonker, C. M., Parton, W. J., Cole, C. V., Flach, K., and Schimel, D. S.: Texture,
719 Climate, and Cultivation Effects on Soil Organic-Matter Content in Us Grassland Soils, Soil Sci
720 Soc Am J, 53, 800-805, 1989.

721 Canadell, J. G., Le Quéré, C., Raupach, M. R., Field, C. B., Buitenhuis, E. T., Ciais, P., Conway,
722 T. J., Gillett, N. P., Houghton, R. A., and Marland, G.: Contributions to accelerating atmospheric
723 CO2 growth from economic activity, carbon intensity, and efficiency of natural sinks,
724 Proceedings of the National Academy of Sciences, 104, 18866-18870, 2007.

725 Caswell, H.: Prospective and retrospective perturbation analyses: their roles in conservation
726 biology, Ecology, 81, 619-627, 2000.

727 Chatfield, C.: Model uncertainty, data mining and statistical-inference, Journal of the Royal
728 Statistical Society Series a-Statistics in Society, 158, 419-466, 1995.

729 Chen, Y., Xia, J., Sun, Z., Li, J., Luo, Y., Gang, C., and Wang, Z.: The role of residence time in
730 diagnostic models of global carbon storage capacity: model decomposition based on a traceable
731 scheme, Scientific reports, 5, 2015.

732 Ciais, P., Gasser, T., Paris, J. D., Caldeira, K., Raupach, M. R., Canadell, J. G., Patwardhan, A.,
733 Friedlingstein, P., Piao, S. L., and Gitz, V.: Attributing the increase in atmospheric CO_2 to
734 emitters and absorbers, Nat Clim Change, 3, 926-930, 2013.

De Kauwe, M. G., Medlyn, B. E., Zaehle, S., Walker, A. P., Dietze, M. C., Hickler, T., Jain, A. K., Luo, Y., Parton, W. J., Prentice, I. C., Smith, B., Thornton, P. E., Wang, S., Wang, Y.-P., Wårlind, D., Weng, E., Crous, K. Y., Ellsworth, D. S., Hanson, P. J., Seok Kim, H., Warren, J. M., Oren, R., and Norby, R. J.: Forest water use and water use efficiency at elevated CO_2: a model-data intercomparison at two contrasting temperate forest FACE sites, Global Change Biology, 19, 1759-1779, 2013.

English, B. P., Min, W., Van Oijen, A. M., Lee, K. T., Luo, G., Sun, H., Cherayil, B. J., Kou, S., and Xie, X. S.: Ever-fluctuating single enzyme molecules: Michaelis-Menten equation revisited, Nature chemical biology, 2, 87-94, 2006.

Exbrayat, J. F., Pitman, A. J., Zhang, Q., Abramowitz, G., and Wang, Y. P.: Examining soil carbon uncertainty in a global model: response of microbial decomposition to temperature, moisture and nutrient limitation, Biogeosciences, 10, 7095-7108, 2013.

Farquhar, G., von Caemmerer, S. v., and Berry, J.: A biochemical model of photosynthetic CO_2 assimilation in leaves of C3 species, Planta, 149, 78-90, 1980.

Fisher, R., McDowell, N., Purves, D., Moorcroft, P., Sitch, S., Cox, P., Huntingford, C., Meir, P., and Ian Woodward, F.: Assessing uncertainties in a second‐generation dynamic vegetation model caused by ecological scale limitations, New Phytol, 187, 666-681, 2010.

Fraser, L. H., Henry, H. A., Carlyle, C. N., White, S. R., Beierkuhnlein, C., Cahill, J. F., Casper, B. B., Cleland, E., Collins, S. L., and Dukes, J. S.: Coordinated distributed experiments: an emerging tool for testing global hypotheses in ecology and environmental science, Frontiers in Ecology and the Environment, 11, 147-155, 2013.

Friedlingstein, P., Cox, P., Betts, R., Bopp, L., Von Bloh, W., Brovkin, V., Cadule, P., Doney, S., Eby, M., Fung, I., Bala, G., John, J., Jones, C., Joos, F., Kato, T., Kawamiya, M., Knorr, W., Lindsay, K., Matthews, H. D., Raddatz, T., Rayner, P., Reick, C., Roeckner, E., Schnitzler, K. G., Schnur, R., Strassmann, K., Weaver, A. J., Yoshikawa, C., and Zeng, N.: Climate-carbon cycle feedback analysis: Results from the (CMIP)-M-4 model intercomparison, J Climate, 19, 3337-3353, 2006.

Goetz, S. J., Bond-Lamberty, B., Law, B. E., Hicke, J. A., Huang, C., Houghton, R. A., McNulty, S., O'Halloran, T., Harmon, M., Meddens, A. J. H., Pfeifer, E. M., Mildrexler, D., and Kasischke, E. S.: Observations and assessment of forest carbon dynamics following disturbance in North America, J Geophys Res-Biogeo, 117, 2012.

Goldbeter, A.: Oscillatory enzyme reactions and Michaelis–Menten kinetics, FEBS letters, 587, 2778-2784, 2013.

Grosse, G., Harden, J., Turetsky, M., McGuire, A. D., Camill, P., Tarnocai, C., Frolking, S., Schuur, E. A. G., Jorgenson, T., Marchenko, S., Romanovsky, V., Wickland, K. P., French, N., Waldrop, M., Bourgeau-Chavez, L., and Striegl, R. G.: Vulnerability of high-latitude soil organic carbon in North America to disturbance, J Geophys Res-Biogeo, 116, 2011.

Hammerling, D. M., Michalak, A. M., and Kawa, S. R.: Mapping of CO_2 at high spatiotemporal resolution using satellite observations: Global distributions from OCO-2, J Geophys Res-Atmos, 117, do6306, 2012.

Hararuk, O., Smith, M. J., and Luo, Y. Q.: Microbial models with data-driven parameters predict stronger soil carbon responses to climate change, Global Change Biology, 21, 2439-2453, 2015.

Hararuk, O., Xia, J. Y., and Luo, Y. Q.: Evaluation and improvement of a global land model against soil carbon data using a Bayesian Markov chain Monte Carlo method, J Geophys Res-Biogeo, 119, 403-417, 2014.

Harley, P., Thomas, R., Reynolds, J., and Strain, B.: Modelling photosynthesis of cotton grown in elevated CO_2, Plant, Cell & Environment, 15, 271-282, 1992.

Hicke, J. A., Allen, C. D., Desai, A. R., Dietze, M. C., Hall, R. J., Hogg, E. H., Kashian, D. M., Moore, D., Raffa, K. F., Sturrock, R. N., and Vogelmann, J.: Effects of biotic disturbances on forest carbon cycling in the United States and Canada, Global Change Biol, 18, 7-34, 2012.

Jenkinson, D., Hart, P., Rayner, J., and Parry, L.: Modelling the turnover of organic matter in long-term experiments at Rothamsted, 1987. 1987.

Jones, C., McConnell, C., Coleman, K., Cox, P., Falloon, P., Jenkinson, D., and Powlson, D.: Global climate change and soil carbon stocks; predictions from two contrasting models for the turnover of organic carbon in soil, Global Change Biol, 11, 154-166, 2005.

Keenan, T. F., Baker, I., Barr, A., Ciais, P., Davis, K., Dietze, M., Dragoni, D., Gough, C. M., Grant, R., Hollinger, D., Hufkens, K., Poulter, B., McCaughey, H., Raczka, B., Ryu, Y., Schaefer, K., Tian, H., Verbeeck, H., Zhao, M., and Richardson, A. D.: Terrestrial biosphere model performance for inter-annual variability of land-atmosphere CO_2 exchange, Global Change Biol, 18, 1971-1987, 2012.

Kloeden, P. E. and Rasmussen, M.: Nonautonomous dynamical systems, American Mathematical Society, 2011.

Kloster, S., Mahowald, N. M., Randerson, J. T., Thornton, P. E., Hoffman, F. M., Levis, S., Lawrence, P. J., Feddema, J. J., Oleson, K. W., and Lawrence, D. M.: Fire dynamics during the 20th century simulated by the Community Land Model, Biogeosciences, 7, 2010.

Le Quéré, C., Moriarty, R., Andrew, R. M., Canadell, J. G., Sitch, S., Korsbakken, J. I., Friedlingstein, P., Peters, G. P., Andres, R. J., Boden, T. A., Houghton, R. A., House, J. I., Keeling, R. F., Tans, P., Arneth, A., Bakker, D. C. E., Barbero, L., Bopp, L., Chang, J., Chevallier, F., Chini, L. P., Ciais, P., Fader, M., Feely, R. A., Gkritzalis, T., Harris, I., Hauck, J., Ilyina, T., Jain, A. K., Kato, E., Kitidis, V., Klein Goldewijk, K., Koven, C., Landschützer, P., Lauvset, S. K., Lefèvre, N., Lenton, A., Lima, I. D., Metzl, N., Millero, F., Munro, D. R., Murata, A., Nabel, J. E. M. S., Nakaoka, S., Nojiri, Y., O'Brien, K., Olsen, A., Ono, T., Pérez, F. F., Pfeil, B., Pierrot, D., Poulter, B., Rehder, G., Rödenbeck, C., Saito, S., Schuster, U., Schwinger, J., Séférian, R., Steinhoff, T., Stocker, B. D., Sutton, A. J., Takahashi, T., Tilbrook, B., van der Laan-Luijkx, I. T., van der Werf, G. R., van Heuven, S., Vandemark, D., Viovy, N.,

Wiltshire, A., Zaehle, S., and Zeng, N.: Global Carbon Budget 2015, Earth Syst. Sci. Data, 7, 349-396, 2015.

Li, J. W., Luo, Y. Q., Natali, S., Schuur, E. A. G., Xia, J. Y., Kowalczyk, E., and Wang, Y. P.: Modeling permafrost thaw and ecosystem carbon cycle under annual and seasonal warming at an Arctic tundra site in Alaska, J Geophys Res-Biogeo, 119, 1129-1146, 2014.

Lloyd, J. and Taylor, J. A.: On the Temperature-Dependence of Soil Respiration, Funct Ecol, 8, 315-323, 1994.

Luo, Y., Ahlström, A., Allison, S. D., Batjes, N. H., Brovkin, V., Carvalhais, N., Chappell, A., Ciais, P., Davidson, E. A., Finzi, A., Georgiou, K., Guenet, B., Hararuk, O., Harden, J. W., He, Y., Hopkins, F., Jiang, L., Koven, C., Jackson, R. B., Jones, C. D., Lara, M. J., Liang, J., McGuire, A. D., Parton, W., Peng, C., Randerson, J. T., Salazar, A., Sierra, C. A., Smith, M. J., Tian, H., Todd-Brown, K. E. O., Torn, M., van Groenigen, K. J., Wang, Y. P., West, T. O., Wei, Y., Wieder, W. R., Xia, J., Xu, X., Xu, X., and Zhou, T.: Toward more realistic projections of soil carbon dynamics by Earth system models, Global Biogeochemical Cycles, 30, 40-56, 2016.

Luo, Y., Weng, E., Wu, X., Gao, C., Zhou, X., and Zhang, L.: Parameter identifiability, constraint, and equifinality in data assimilation with ecosystem models, Ecological Applications, 19, 571-574, 2009.

Luo, Y. and Zhou, X.: Soil respiration and the environment, Academic Press, Burlington, MA, USA, 2006.

Luo, Y. Q., Keenan, T. F., and Smith, M.: Predictability of the terrestrial carbon cycle, Global Change Biol, 21, 1737-1751, 2015.

Luo, Y. Q., Ogle, K., Tucker, C., Fei, S. F., Gao, C., LaDeau, S., Clark, J. S., and Schimel, D. S.: Ecological forecasting and data assimilation in a data-rich era, Ecol Appl, 21, 1429-1442, 2011.

Luo, Y. Q. and Weng, E. S.: Dynamic disequilibrium of the terrestrial carbon cycle under global change, Trends Ecol Evol, 26, 96-104, 2011.

Luo, Y. Q., White, L. W., Canadell, J. G., DeLucia, E. H., Ellsworth, D. S., Finzi, A. C., Lichter, J., and Schlesinger, W. H.: Sustainability of terrestrial carbon sequestration: A case study in Duke Forest with inversion approach, Global Biogeochem Cy, 17, 2003.

Luo, Y.Q., Wu, L., Andrews, J.A., White, L., Matamala, R., Schafer, K.V.R., and Schlesinger, W. H. Elevated CO2 differentiates ecosystem carbon processes: Deconvolution analysis of Duke Forest FACE data.. Ecological Monographs. **71**:357-376, 2001.

Manzoni, S. and Porporato, A.: Soil carbon and nitrogen mineralization: theory and models across scales, Soil Biology and Biochemistry, 41, 1355-1379, 2009.

Matamala, R., Jastrow, J. D., Miller, R. M., and Garten, C. T.: Temporal changes in C and N stocks of restored prairie: Implications for C sequestration strategies, Ecological Applications, 18, 1470-1488, 2008.

Medlyn, B. E., Zaehle, S., De Kauwe, M. G., Walker, A. P., Dietze, M. C., Hanson, P. J., Hickler, T., Jain, A. K., Luo, Y., Parton, W., Prentice, I. C., Thornton, P. E., Wang, S., Wang, Y.-P., Weng, E., Iversen, C. M., McCarthy, H. R., Warren, J. M., Oren, R., and Norby, R. J.: Using ecosystem experiments to improve vegetation models, Nature Climate Change, 5, 528-534, 2015.

Moorcroft, P., Hurtt, G., and Pacala, S. W.: A method for scaling vegetation dynamics: the ecosystem demography model (ED), Ecol Monogr, 71, 557-586, 2001.

Oleson, K., Lawrence, D., Bonan, G., Drewniak, B., Huang, M., Koven, C., Levis, S., Li, F., Riley, W., and Subin, Z.: Technical description of version 4.5 of the Community Land Model (CLM), National Center for Atmospheric Research, Boulder, Colorado, 2013.

Olson, J. S.: Energy storage and the balance of producers and decomposers in ecological systems, Ecology, 44, 322-331, 1963.

Pan, Y., Birdsey, R. A., Phillips, O. L., and Jackson, R. B.: The structure, distribution, and biomass of the world's forests, Annual Review of Ecology, Evolution, and Systematics, 44, 593-622, 2013.

Parolari A., Porporato A., Forest soil carbon and nitrogen cycles under biomass harvest: stability, transient response, and feedback. *Ecological Modelling*, 329, 64-76, 2016

Parton, W. J., Schimel, D. S., Cole, C. V., and Ojima, D. S.: Analysis of Factors Controlling Soil Organic-Matter Levels in Great-Plains Grasslands, Soil Sci Soc Am J, 51, 1173-1179, 1987.

Parton, W. J., Scurlock, J. M. O., Ojima, D. S., Gilmanov, T. G., Scholes, R. J., Schimel, D. S., Kirchner, T., Menaut, J. C., Seastedt, T., Moya, E. G., Kamnalrut, A., and Kinyamario, J. I.: Observations and Modeling of Biomass and Soil Organic-Matter Dynamics for the Grassland Biome Worldwide, Global Biogeochem Cy, 7, 785-809, 1993.

Parton, W. J., Stewart, J. W. B., and Cole, C. V.: Dynamics of C, N, P and S in Grassland Soils - a Model, Biogeochemistry, 5, 109-131, 1988.

Potter, C. S., Randerson, J. T., Field, C. B., Matson, P. A., Vitousek, P. M., Mooney, H. A., and Klooster, S. A.: Terrestrial Ecosystem Production: a Process Model-Based on Global Satellite and Surface Data, Global Biogeochem Cy, 7, 811-841, 1993.

Prentice, I. C., Kelley, D. I., Foster, P. N., Friedlingstein, P., Harrison, S. P., and Bartlein, P. J.: Modeling fire and the terrestrial carbon balance, Global Biogeochem Cy, 25, 2011.

Purves, D. and Pacala, S.: Predictive models of forest dynamics, Science, 320, 1452-1453, 2008.

Rafique, R., Xia, J., Hararuk, O., and Luo, Y.: Structural analysis of three global land models on carbon cycle simulations using a traceability framework, Biogeosciences Discussions, 11, 9979-10014, 2014.

881 Rustad, L., Campbell, J., Marion, G., Norby, R., Mitchell, M., Hartley, A., Cornelissen, J., and
882 Gurevitch, J.: A meta-analysis of the response of soil respiration, net nitrogen mineralization,
883 and aboveground plant growth to experimental ecosystem warming, Oecologia, 126, 543-562,
884 2001.

885 Schwalm, C. R., Williams, C. A., Schaefer, K., Anderson, R., Arain, M. A., Baker, I., Barr, A.,
886 Black, T. A., Chen, G., Chen, J. M., Ciais, P., Davis, K. J., Desai, A., Dietze, M., Dragoni, D.,
887 Fischer, M. L., Flanagan, L. B., Grant, R., Gu, L., Hollinger, D., Izaurralde, R. C., Kucharik, C.,
888 Lafleur, P., Law, B. E., Li, L., Li, Z., Liu, S., Lokupitiya, E., Luo, Y., Ma, S., Margolis, H.,
889 Matamala, R., McCaughey, H., Monson, R. K., Oechel, W. C., Peng, C., Poulter, B., Price, D. T.,
890 Riciutto, D. M., Riley, W., Sahoo, A. K., Sprintsin, M., Sun, J., Tian, H., Tonitto, C., Verbeeck,
891 H., and Verma, S. B.: A model-data intercomparison of CO_2 exchange across North America:
892 Results from the North American Carbon Program site synthesis, Journal of Geophysical
893 Research: Biogeosciences, 115, n/a-n/a, 2010.

894 Sellers, P. J., Bounoua, L., Collatz, G. J., Randall, D. A., Dazlich, D. A., Los, S. O., Berry, J. A.,
895 Fung, I., Tucker, C. J., Field, C. B., and Jensen, T. G.: Comparison of radiative and physiological
896 effects of doubled atmospheric CO_2 on climate, Science, 271, 1402-1406, 1996.

897 Schädel, C, Schuur, E. A. G., Bracho R., Elberling, B., Knoblauch, C, Lee, H, Luo, Y.Q.,
898 Shaver, G. R., Turetsky, M. R. Circumpolar assessment of permafrost C quality and its
899 vulnerability over time using long-term incubation data. Global Change Biology, **20**: 641–652,
900 2014.

901 Shi, Z., Yang, Y., Zhou, X., Weng, E., Finzi, A. C., and Luo, Y.: Inverse analysis of coupled
902 carbon–nitrogen cycles against multiple datasets at ambient and elevated CO2, J Plant Ecol, 9,
903 285-295, 2016.

904 Sierra, C. A. and Müller, M.: A general mathematical framework for representing soil organic
905 matter dynamics, Ecol Monogr, 85, 505-524, 2015.

906 Smith, J. U., Smith, P., Monaghan, R., and MacDonald, J.: When is a measured soil organic
907 matter fraction equivalent to a model pool?, Eur J Soil Sci, 53, 405-416, 2002.

908 Smith, P., Davis, S. J., Creutzig, F., Fuss, S., Minx, J., Gabrielle, B., Kato, E., Jackson, R. B.,
909 Cowie, A., and Kriegler, E.: Biophysical and economic limits to negative CO_2 emissions, Nat
910 Clim Change, 6, 42-50, 2016.

911 Stewart, C. E., Plante, A. F., Paustian, K., Conant, R. T., and Six, J.: Soil carbon saturation:
912 Linking concept and measurable carbon pools, Soil Sci Soc Am J, 72, 379-392, 2008.

913 Thonicke, K., Spessa, A., Prentice, I., Harrison, S. P., Dong, L., and Carmona-Moreno, C.: The
914 influence of vegetation, fire spread and fire behaviour on biomass burning and trace gas
915 emissions: results from a process-based model, Biogeosciences, 7, 1991-2011, 2010.

916 Tian, H. Q., Yang, Q. C., Najjar, R. G., Ren, W., Friedrichs, M. A. M., Hopkinson, C. S., and
917 Pan, S. F.: Anthropogenic and climatic influences on carbon fluxes from eastern North America

to the Atlantic Ocean: A process-based modeling study, J Geophys Res-Biogeo, 120, 752-772, 2015.

Todd-Brown, K. E. O., Randerson, J. T., Post, W. M., Hoffman, F. M., Tarnocai, C., Schuur, E. A. G., and Allison, S. D.: Causes of variation in soil carbon simulations from CMIP5 Earth system models and comparison with observations, Biogeosciences, 10, 1717-1736, 2013.

Walker, A. P., Aranda, I., Beckerman, A. P., Bown, H., Cernusak, L. A., Dang, Q. L., Domingues, T. F., Gu, L., Guo, S., Han, Q., Kattge, J., Kubiske, M., Manter, D., Merilo, E., Midgley, G., Porte, A., Scales, J. C., Tissue, D., Turnbull, T., Warren, C., Wohlfahrt, G., Woodward, F. I., and Wullschleger, S. D.: A Global Data Set of Leaf Photosynthetic Rates, Leaf N and P, and Specific Leaf Area. Data set. Available on-line [http://daac.ornl.gov] from Oak Ridge National Laboratory Distributed Active Archive Center, Oak Ridge, Tennessee, USA. http://dx.doi.org/10.3334/ORNLDAAC/1224, 2014. 2014.

Wang, G. B., Zhou, Y., Xu, X., Ruan, H. H., and Wang, J. S.: Temperature Sensitivity of Soil Organic Carbon Mineralization along an Elevation Gradient in the Wuyi Mountains, China, Plos One, 8, 2013.

Wang, Y.-P. and Leuning, R.: A two-leaf model for canopy conductance, photosynthesis and partitioning of available energy I:: Model description and comparison with a multi-layered model, Agricultural and Forest Meteorology, 91, 89-111, 1998.

Wang, Y., Jiang, J., Chen-Charpentier, B., Agusto, F., Hastings, A., Hoffman, F., Rasmussen, M., Smith, M., Todd-Brown, K., and Wang, Y.: Responses of two nonlinear microbial models to warming and increased carbon input, Biogeosciences, 13, 887-902, 2016.

Wang, Y. P., Chen, B. C., Wieder, W. R., Leite, M., Medlyn, B. E., Rasmussen, M., Smith, M. J., Agusto, F. B., Hoffman, F., and Luo, Y. Q.: Oscillatory behavior of two nonlinear microbial models of soil carbon decomposition, Biogeosciences, 11, 1817-1831, 2014.

Weng, E. S. and Luo, Y. Q.: Soil hydrological properties regulate grassland ecosystem responses to multifactor global change: A modeling analysis, J Geophys Res-Biogeo, 113, 2008.

Weng, E. S., Malyshev, S., Lichstein, J. W., Farrior, C. E., Dybzinski, R., Zhang, T., Shevliakova, E., and Pacala, S. W.: Scaling from individual trees to forests in an Earth system modeling framework using a mathematically tractable model of height-structured competition, Biogeosciences, 12, 2655-2694, 2015.

Weng, E. S. S., Luo, Y. Q., Wang, W. L., Wang, H., Hayes, D. J., McGuire, A. D., Hastings, A., and Schimel, D. S.: Ecosystem carbon storage capacity as affected by disturbance regimes: A general theoretical model, J Geophys Res-Biogeo, 117, 2012.

West, T. O., Bandaru, V., Brandt, C. C., Schuh, A., and Ogle, S.: Regional uptake and release of crop carbon in the United States, Biogeosciences, 8, 2037-2046, 2011.

Wieder, W. R., Bonan, G. B., and Allison, S. D.: Global soil carbon projections are improved by modelling microbial processes, Nat Clim Change, 3, 909-912, 2013.

Xia, J. Y., Luo, Y. Q., Wang, Y. P., and Hararuk, O.: Traceable components of terrestrial carbon storage capacity in biogeochemical models, Global Change Biol, 19, 2104-2116, 2013.

Xie, X. S.: Enzyme kinetics, past and present, Science, 342, 1457-1459, 2013.

Xu, X., Luo, Y. Q., and Zhou, J. Z.: Carbon quality and the temperature sensitivity of soil organic carbon decomposition in a tallgrass prairie, Soil Biol Biochem, 50, 142-148, 2012.

Xu, X., Shi, Z., Li, D., Rey, A., Ruan, H. H., Craine, J. M., Liang, J., Zhou, J., and Luo, Y.: Soil properties control decomposition of soil organic carbon: Results from data-assimilation analysis, Geoderma, 262, 235-242, 2016.

Yang, Y. H., Luo, Y. Q., and Finzi, A. C.: Carbon and nitrogen dynamics during forest stand development: a global synthesis, New Phytol, 190, 977-989, 2011.

Zhang, D. Q., Hui, D. F., Luo, Y. Q., and Zhou, G. Y.: Rates of litter decomposition in terrestrial ecosystems: global patterns and controlling factors, J Plant Ecol, 1, 85-93, 2008.

968 **Fig. 1** The Terrestrial ECOsystem (TECO) model and its outputs. Panel a is a schematic
969 representation of C transfers among multiple pools in plant, litter and soil in the TECO model.
970 TECO has feedback loops of C among soil pools. CWD = coarse wood debris, SOM = Soil
971 Organic Matter. Panel b compares the original TECO model outputs with those from matrix
972 equations for net ecosystem production (NEP = the sum of elements in $X'(t)$ from eq. 1). The
973 perfect match between the TECO outputs and NEP from eq. 1 is due to the fact that they are
974 mathematically equivalent. Panel c compares the original TECO model outputs with those from
975 matrix equations for ecosystem C storage (= the sum of elements in $X(t)$ from eq. 2). The C
976 storage values calculated with eq. 2 are close to 1:1 line with r^2 =0.998 with the modeled values
977 (panel c). The minor mismatch in estimated C storage between the matrix equation calculation
978 and TECO outputs is due to numerical errors via inverse matrix operation with some small
979 numbers.
980
981 **Fig. 2** Seasonal cycles of the C storage capacity and C storage dynamics for the leaf pool (i.e.,
982 pool 1 as shown in Fig. 1). All the components are showed in panels b-d to calculate $x_{c,1}(t) =$
983 $b_1 u(t)\tau_1$ through multiplication, where $u(t) = NPP$ and $\tau_1 = 1/k_1$ for leaf.
984
985 **Fig. 3** Seasonal cycles of the C storage capacity and C storage dynamics for the litter pool (i.e.,
986 pool 4 as shown in Fig. 1). All the components are showed to calculate
987 $x_{c,4,u}(t) = \sum_{j=1}^{n} f_{4j}\,\tau_4 b_j u(t)$ in panels b-e and $x_{c,4,p}(t) = \sum_{j=1,j\neq 4}^{n} f_{4j}\,\tau_4 x'_j(t)$ in panels f-i for
988 litter. $x_{c,4,u}(t)$ is the maximal amount of C that can transfer from C input to the litter pool.
989 $x_{c,4,p}(t)$ is the maximal amount of C that can transfer from all the other pools to the litter pool.
990 This figure is to illustrate the network of pools through which C is distributed.

991

992 **Fig. 4** Components of the C storage capacity for litter pool (i.e., pool 4 as shown in Fig. 1).
993 Component, $x_{c,4,u}(t)$, is the C from C input and component, $x_{c,4,p}(t)$, is the C from all the other
994 pools to the litter pool. The sum of them is the attractor that determines the direction of C storage
995 change in pool 4.

996

997 **Fig. 5** Transient dynamics of ecosystem C storage in response to global change in Harvard
998 Forest. Panel a shows the time courses of the ecosystem C storage capacity, the ecosystem C
999 storage potential, and ecosystem C storage (i.e., C stock) from 1850 to 2100. Panel b shows time
1000 courses of NPP(t) as C input and ecosystem residence times. Panel c shows correlated changes in
1001 ecosystem C storage potential and net ecosystem production (NEP). Panel d illustrates the
1002 regression between the C storage potential and NEP.

1003

1004 **Fig. 6** The C storage capacity ($x_{c,i}(t)$), the C storage potential ($x_{p,i}(t)$), and C storage ($x_i(t)$) of
1005 individual pools. The potential is nearly zero for those fast turnover pools with short residence
1006 times but very large for those pools with long residence times.

1007

1008 **Fig. 7** The C storage potential of individual pools ($x_{p,i}$) as influenced by net C pool change of
1009 different pools (x'_i) in their corresponding rows. The correlation coefficients show the degree of
1010 influences of net C pool change in one pool on the C storage potential of the corresponding pool
1011 through the network of C transfer. Those empty cells indicate no pathways of C transfer between
1012 those pools as indicated in Fig. 1.

1013

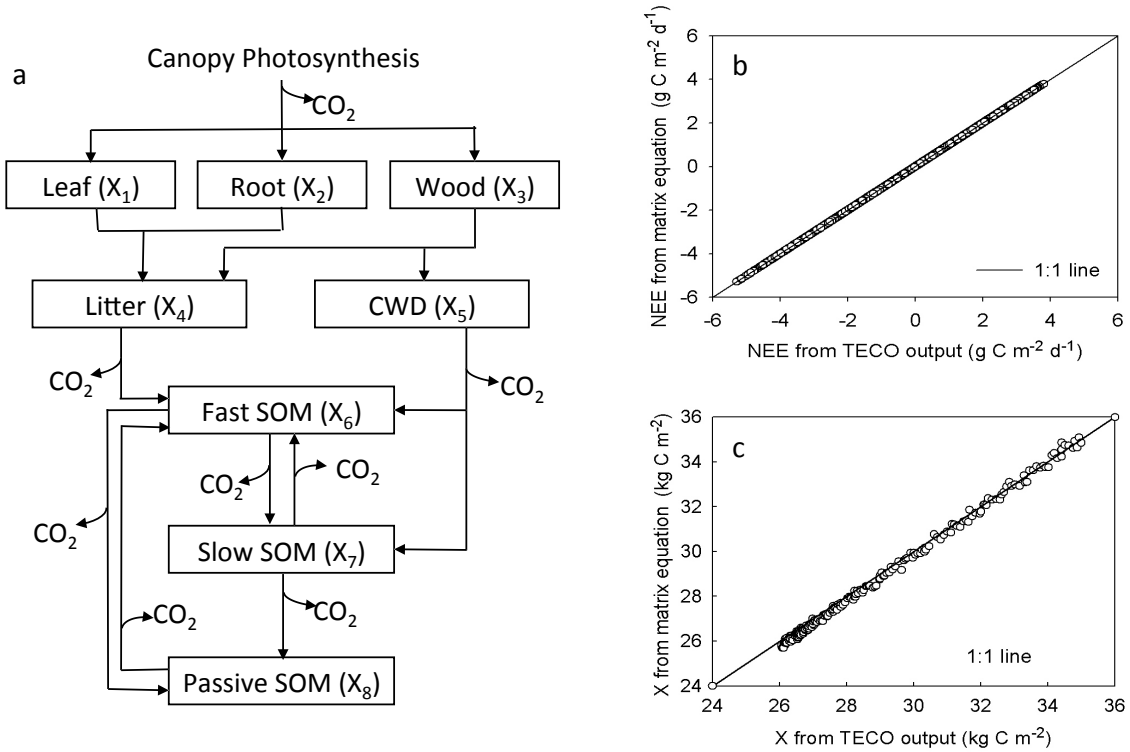
a
Canopy Photosynthesis
CO2
Leaf (X1)
Root (X2)
Wood (X3)
Litter (X4)
CWD (X5)
Fast SOM (X6)
Slow SOM (X7)
Passive SOM (X8)
b
NEE from matrix equation (g C m-2 d-1)
NEE from TECO output (g C m-2 d-1)
1:1 line
c
X from matrix equation (kg C m-2)
X from TECO output (kg C m-2)
1:1 line

Fig. 1

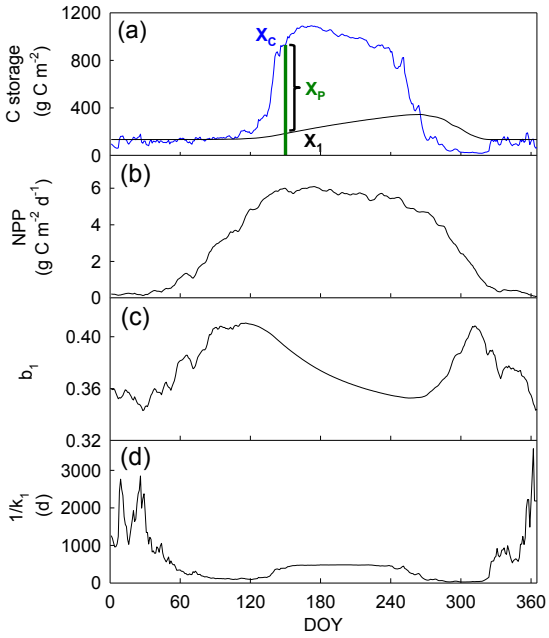
(a)
X_C
X_P
X_1
C storage (g C m^{-2})
1200
800
400
0
(b)
NPP (g C m^{-2} d^{-1})
6
4
2
0
(c)
b_1
0.40
0.36
0.32
(d)
$1/k_1$ (d)
3000
2000
1000
0
0
60
120
180
240
300
360
DOY

Fig. 2

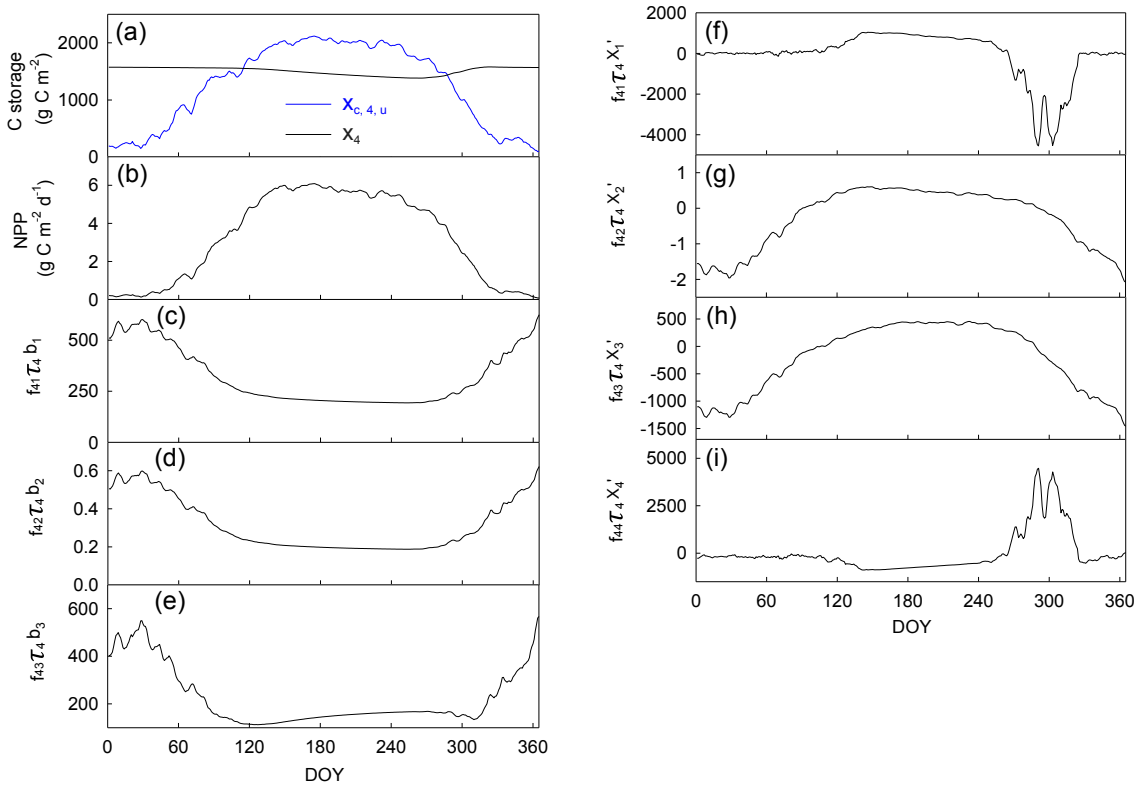

1023
1024

Fig. 3

1025
1026

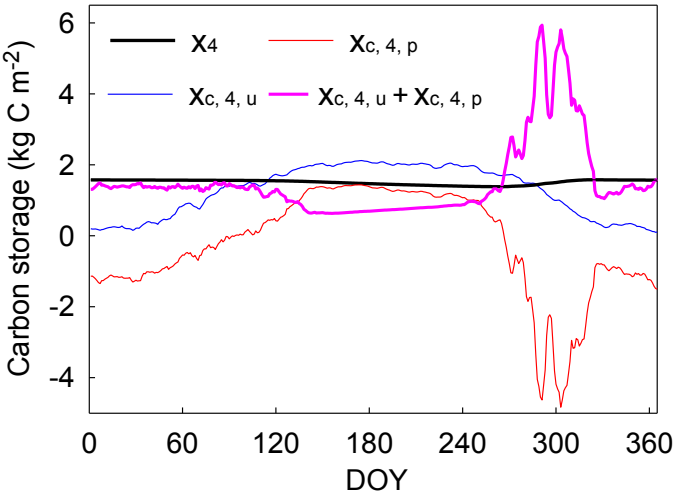

1027
1028
1029 Fig. 4

1030

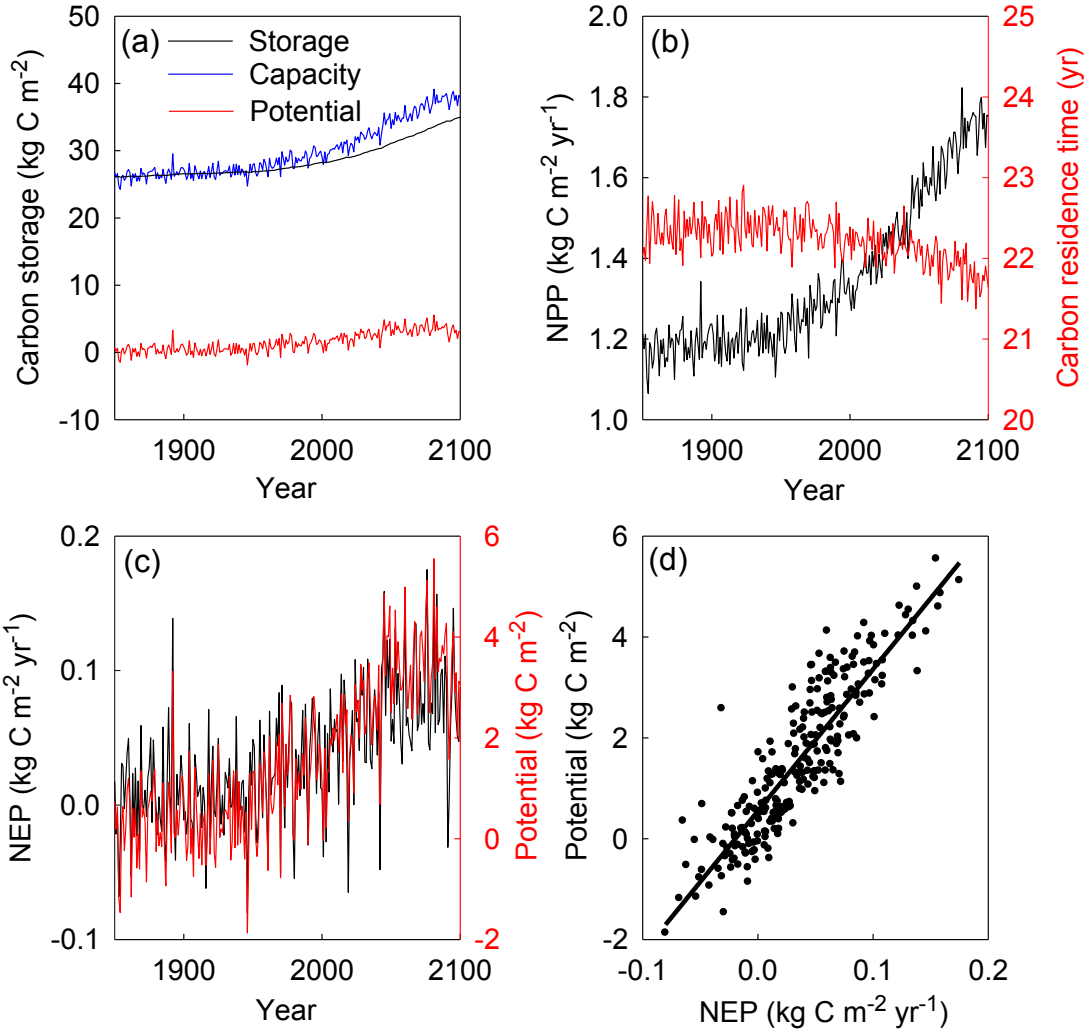

1031
1032
1033 Fig. 5
1034
1035

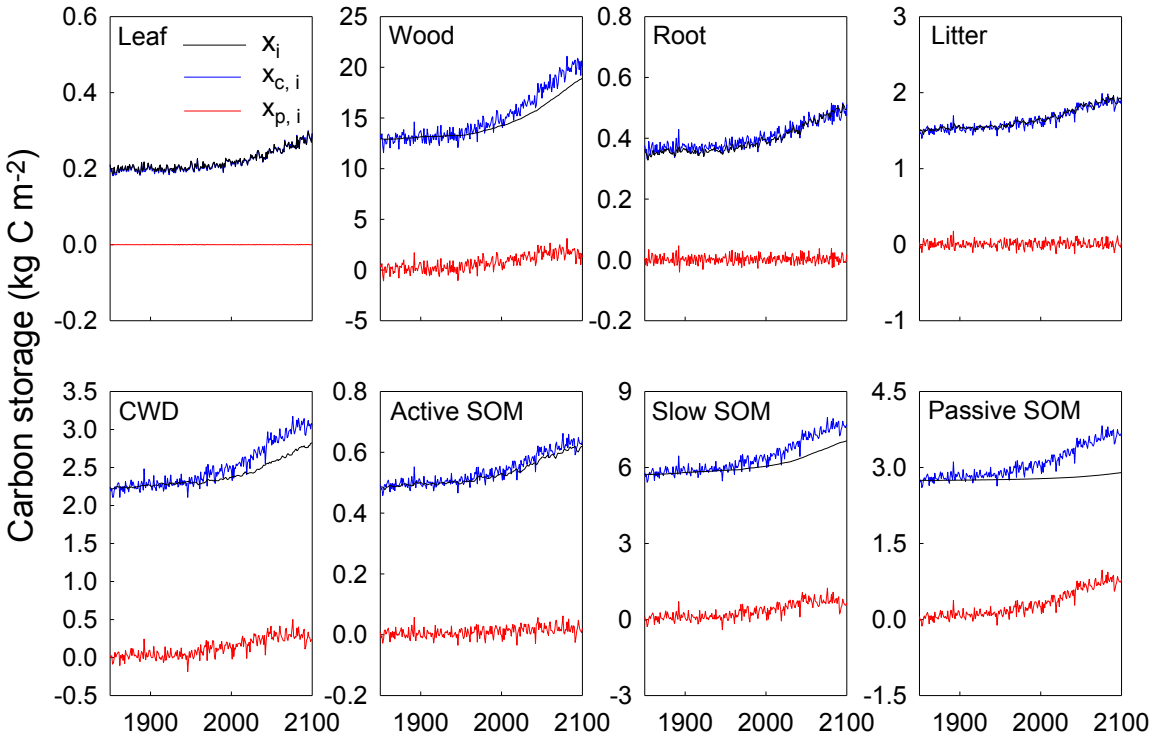
Carbon storage (kg C m-2)
Leaf
xi
xc, i
xp, i
Wood
Root
Litter
CWD
Active SOM
Slow SOM
Passive SOM
1900
2000
2100

Fig. 6

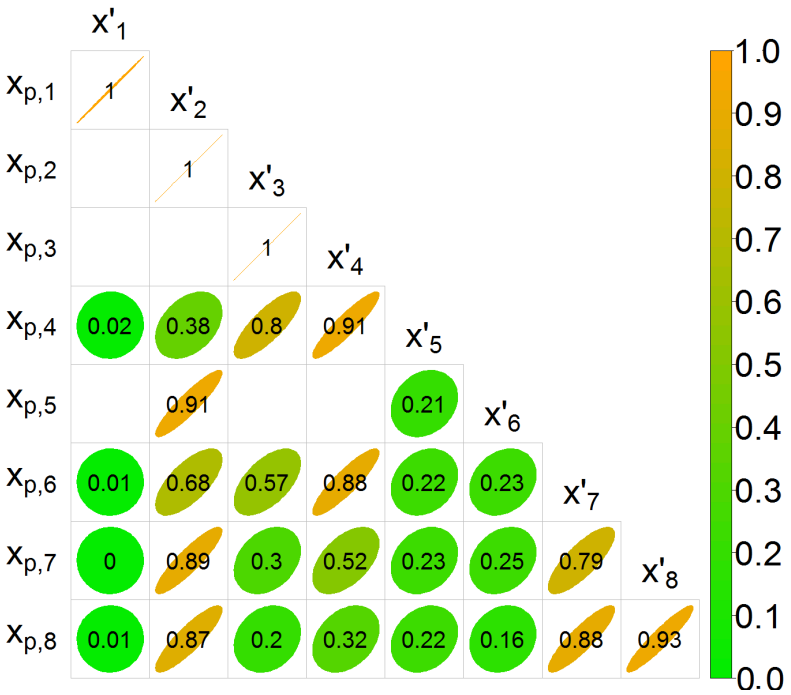
x'1
x'2
x'3
x'4
x'5
x'6
x'7
x'8
xp,1
xp,2
xp,3
xp,4
xp,5
xp,6
xp,7
xp,8
1
1
1
0.02
0.38
0.8
0.91
0.91
0.21
0.01
0.68
0.57
0.88
0.22
0.23
0
0.89
0.3
0.52
0.23
0.25
0.79
0.01
0.87
0.2
0.32
0.22
0.16
0.88
0.93
1.0
0.9
0.8
0.7
0.6
0.5
0.4
0.3
0.2
0.1
0.0

Fig. 7